Al_2O_3 miroring resonators as a novel refractive index sensor platform

M. de Goede,[1] M. Dijkstra,[1] J. Ramón-Azcón,[2] E. M. Fraiz,[2] S. M. García Blanco[1]

[1] Optical Sciences Group, MESA+ Institute for Nanotechnology, University of Twente, P.O. Box 217, 7500 AE Enschede, The Netherlands
[2] Biomimetic Systems for Cell Engineering, Institute for Bioengineering of Catalonia, University of Barcelona, C/ Baldiri Reixac 15-21, 08028 Barcelona, Spain
e-mail: m.degoede@utwente.nl

Microring resonators are of great interest for refractive index sensors. Traditionally, they are realized on a SOI, Si_3N_4 or SiON platform. Al_2O_3 is an interesting alternative platform for optical refractive index sensors, since it can incorporate gain by rare-earth ion doping. This could compensate for the resonator losses and increase their sensitivity. Here, we present undoped Al_2O_3 microring resonators with a quality factor of 35000 that can be used as both a bulk refractive index sensor and a surface sensor.

Introduction

Microring resonators are excellent candidates for label-free biosensors due to their high quality factor, strong optical interaction with the analyte, and the capability of large-scale microfabrication [1]. High sensitivities for both bulk and surface sensing were previously demonstrated on the Si [2], Si_3N_4 [3], and SiON [4] passive platforms. Alternatively, active platforms such as rare-earth ion doped glasses can be used for whispering gallery resonator based sensors and have the possibility of on-chip signal generation for ease of detection [5]. Both microring resonator lasers [6] and laser-based sensors [7] have been already realized in the Al_2O_3 waveguide platform. Here, undoped planar integrated passive Al_2O_3 microring resonators are presented as evanescent field sensors towards the realization of ultra-sensitive, on-chip active microring resonator biosensors.

Sensor Design and Fabrication

The geometrical parameters of a microring resonator are the waveguide cross section, the microring bend radius and the width and length of the coupling gap between bus waveguide and microring. These parameters were optimized with a finite element mode solver based on the criteria of single mode condition, minimum round-trip losses, corresponding critical coupling and highest possible quality factor for a central wavelength $\lambda = 1550$ nm. The designed parameters are a waveguide cross section of $2\times0.6\,\mu m^2$, a bend radius of 200 µm, a coupling gap of 1.4 µm and a coupling length of 70 µm for critical coupling for an under cladding of SiO_2 and an upper cladding of H_2O. The fundamental transverse mode of the optimal waveguide cross section is shown in Figure 1(a) and these optimal geometrical parameters would correspond with a quality-factor of 70e3.
Operation of the microring resonator as a sensor is based on the spectral shift of the resonances [8]. The transmission spectrum of the device exhibits Lorentzian resonances whenever the round-trip phase of the light travelling in the microring equals an integer

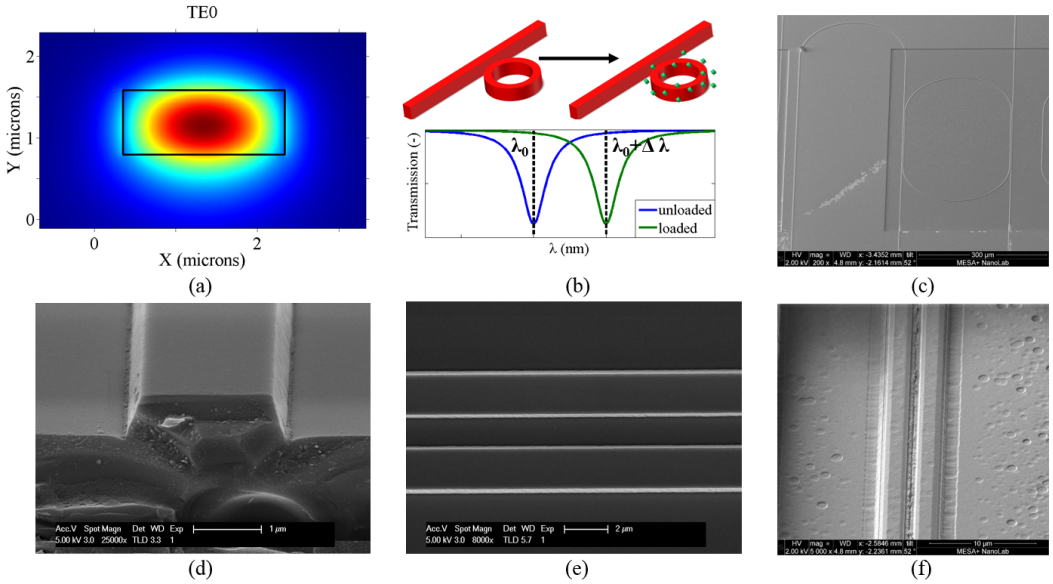

Figure 1: (a) Optimized waveguide cross section with the x-component of the electric field of the fundamental mode, (b) microring resonator sensing principle, (c) Al_2O_3 micoring resonator with a sensing window etched in the SiO_2 cladding, (d) uncladded Al_2O_3 waveguide, (e) the uncladded coupling gap consisting out of two waveguides, (f) coupling gap in sensing window consisting out of two waveguides with roughness in the gap.

multiple of 2π. Whenever the evanescent modal field probes an environmental perturbation surrounding the ring, a change in the accumulated round-trip phase is induced , resulting in a shift in resonance wavelength, as shown in Figure 1(b).
Fabrication of the sensor starts with the sputter deposition of stoichiometric dielectric Al_2O_3 layers on a SiO_2 substrate with an AJA ATC 1500 sputter coater. Subsequently, waveguides and microring resonators are defined with UV lithography and etched with an Oxford Plasmalab System 100 inductively coupled plasma reactive ion etcher. Then, a SiO_2 cladding is deposited with PECVD in which sensing windows were etched. Finally, the wafer was diced into small chips ($2.5\times0.5\,mm^2$) containing the devices. Figures 1(c)–(f) show the final structures after fabrication. The difference between Figure 1(e) and 1(f) arises from the SiO_2 etching, which induces roughness in and around the coupling section initially absent.

Results

Transmission spectra of the devices were acquired with an Agilent 81646 tunable laser in the wavelength range $\lambda = 1530$–$1550\,nm$ at a resolution of 1 pm. TE-polarized laser light was guided through a single-mode, polarization maintaining fiber and butt-coupled to the chip by using an index-matching fluid. The transmitted light was coupled out similarly and guided to a photodiode. Figure 2(a) displays a typical transmission spectrum of a microring resonator with a SiO_2 cladding.
After acquisition the spectra are analyzed for extraction of the parameters of the microring resonator such as the free spectral range, finesse, and quality factor. First, the location of the resonance wavelengths were determined in the transmission spectrum. This was followed by normalization of the data to unity. The normalized response of the ring

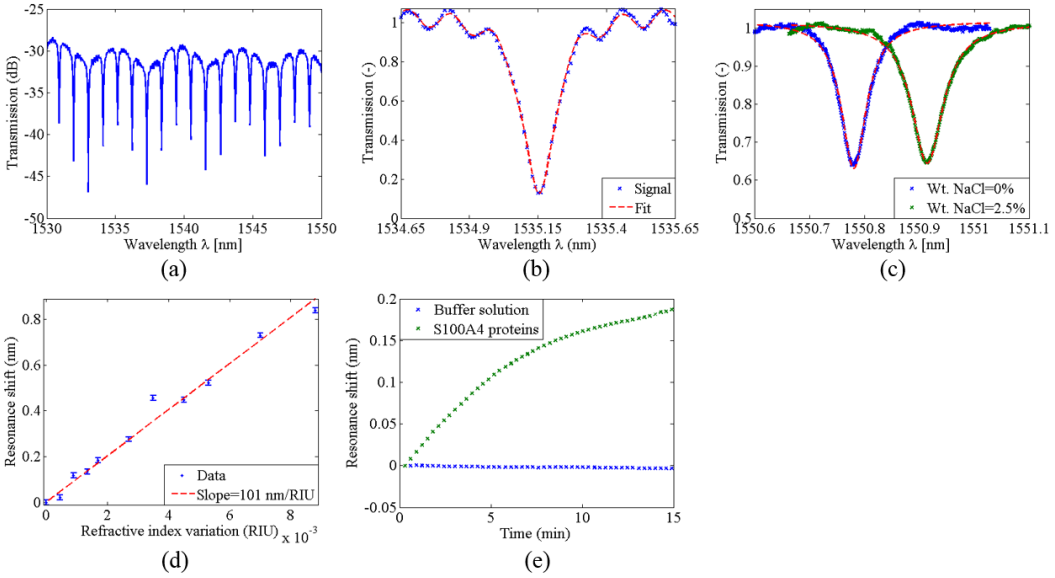

Figure 2: (a) Transmission spectrum of a microring resonator with a SiO_2 upper cladding (b). Lorentzian plus sinusoidal fit. (c). Resonance shift induced by saline concentrations. (d). Bulk sensitivity measurement. (e). Attachment of S100A4 proteins on the sensor's surface.

around the resonance wavelength 1535.15 nm is shown in Figure 2(b), where the notch is the microring's resonance and the sinusoidal fluctuations at either side are Fabry-Pérot reflections within the device. The latter is fitted with a sinusoidal function, the former with a Lorentzian function from which the location of the resonance wavelength, the Lorentzian linewidth, and the extinction ratio were determined. These were used to calculate the previously mentioned parameters together with the group index and self-coupling and round trip loss coefficients of the microring. Applying this procedure to the spectra of Figures 2(a) and (b) yields a free-spectral-range of 1.1 nm, a finesse of 8, a quality-factor of 12e3, a group index of 1.60, a self-coupling coefficient of 0.76 and round trip loss of 1.1 dB. Finally, this fitting routine can be repeated for the sensor experiments to reliably determine the location of the resonance wavelengths, allowing for the precise determination of environmentally induced resonance wavelength shifts.

On a microring resonator with the sensing window opened bulk sensitivity measurements were performed. The device has a finesse of 23 and a quality-factor of 35e3, resulting from being under coupled due to the lower refractive index of H_2O compared to SiO_2, which was the cladding considered in the design. Sensor experiments were performed by dropping NaCl solutions droplets with varying concentrations on the sensing window. For each concentration, the resonance peak was fitted to accurately determine its location, as shown in Figures 2(c) and (d). The slope sensitivity S was determined at $S = 101$ nm/RIU, and the limit of detection (LOD) at 3e-4 RIU. The latter was determined by $\mathrm{LOD} = 3\sigma/S$, where σ is the smallest reliably detectable resonance wavelength shift. The LOD is rather high due to a $\sigma = 10$ pm standard deviation of the resonance wavelength shift for repeated wetting and drying experiments, which could be reduced significantly by integrating the device with microfluidics and temperature control on the stage.

Finally, surface sensing experiments were performed on the same device to demonstrate the possibility of using Al_2O_3 for biosensing experiments. These were focussed on the

detection of the S100A4 protein, which is associated with human tumour development [9]. After cleaning the chip it was immersed in a 0.1% v/v of silane and PBS, followed by incubation of a 10 µg/l S100A4 antibodies in PBS, to which S100A4 binds selectively. Then, a droplet of 1.7 µM S100A4 in PBS was added to the device while the drift in resonance wavelength was monitored for 15 minutes. Figure 2(e) shows this drift associated with binding of S100A4 to the antibodies compared with the drift of plain PBS, indicating that the drift is due to the attachment of the analyte to the microring resonator's surface. A binding slope of 25 nm/min was observed.

Conclusions and Outlook

Al_2O_3 microring resonators were presented as a novel refractive index sensor platform for both bulk refractive index and surface sensing. Preliminary results have shown a bulk sensitivity of 101 nm/RIU, together with the detection of 1.7 µM S100A4 through the binding of the proteins to the device's surface functionalized with antibodies. The latter demonstrates the potential of the Al_2O_3 platform for disease diagnosis. Future work will include improving the sensor stability by introducing microfluidics and temperature control, and the inclusion of rare-earth ion doping for the realization of active optical biosensors integrated on the chip.

Acknowledgement

This project has received funding from the European Union's Horizon 2020 research and innovation programme under grant agreement No 634928.

References

[1] Y. Sun and X. Fan, "Optical ring resonators for biochemical and chemical sensing," *Analytical and bioanalytical chemistry*, vol. 399, no. 1, pp. 205–211, 2011.

[2] M. Iqbal, M. A. Gleeson, B. Spaugh, F. Tybor, W. G. Gunn, M. Hochberg, T. Baehr-Jones, R. C. Bailey, and L. C. Gunn, "Label-free biosensor arrays based on silicon ring resonators and high-speed optical scanning instrumentation," *IEEE Journal of Selected Topics in Quantum Electronics*, vol. 16, no. 3, pp. 654–661, 2010.

[3] R. Heideman, M. Hoekman, and E. Schreuder, "Triplex-based integrated optical ring resonators for lab-on-a-chip and environmental detection," *IEEE Journal of Selected Topics in Quantum Electronics*, vol. 18, no. 5, pp. 1583–1596, 2012.

[4] A. Samusenko, D. Gandolfi, G. Pucker, T. Chalyan, R. Guider, M. Ghulinyan, and L. Pavesi, "A sion microring resonator-based platform for biosensing at 850 nm," *Journal of Lightwave Technology*, vol. 34, no. 3, pp. 969–977, 2016.

[5] L. He, Ş. K. Özdemir, J. Zhu, W. Kim, and L. Yang, "Detecting single viruses and nanoparticles using whispering gallery microlasers," *Nature nanotechnology*, vol. 6, no. 7, pp. 428–432, 2011.

[6] J. Bradley, R. Stoffer, L. Agazzi, F. Ay, K. Wörhoff, and M. Pollnau, "Integrated al2o3:er3+ ring lasers on silicon with wide wavelength selectivity," *Optics letters*, vol. 35, no. 1, pp. 73–75, 2010.

[7] E. H. Bernhardi, K. O. Werf, A. J. Hollink, K. Wörhoff, R. M. Ridder, V. Subramaniam, and M. Pollnau, "Intra-laser-cavity microparticle sensing with a dual-wavelength distributed-feedback laser," *Laser & photonics reviews*, vol. 7, no. 4, pp. 589–598, 2013.

[8] K. De Vos, I. Bartolozzi, E. Schacht, P. Bienstman, and R. Baets, "Silicon-on-insulator microring resonator for sensitive and label-free biosensing," *Optics express*, vol. 15, no. 12, pp. 7610–7615, 2007.

[9] K. Boye and G. M. Mælandsmo, "S100a4 and metastasis: a small actor playing many roles," *The American journal of pathology*, vol. 176, no. 2, pp. 528–535, 2010.